# Development of online separation and surfactant quantification in effluents from an enhanced oil recovery (EOR) experiment

Elie Ayoub, Perrine Cologon, Marie Marsiglia, Jean-Baptiste Salmon, Christine Dalmazzone

▶ **To cite this version:**

Elie Ayoub, Perrine Cologon, Marie Marsiglia, Jean-Baptiste Salmon, Christine Dalmazzone. Development of online separation and surfactant quantification in effluents from an enhanced oil recovery (EOR) experiment. Journal of Petroleum Science and Engineering, 2022, 208 (Part D), pp.109696. 10.1016/j.petrol.2021.109696 . hal-03426472

**HAL Id: hal-03426472**
**https://hal.science/hal-03426472**

Submitted on 12 Nov 2021

**HAL** is a multi-disciplinary open access archive for the deposit and dissemination of scientific research documents, whether they are published or not. The documents may come from teaching and research institutions in France or abroad, or from public or private research centers.

L'archive ouverte pluridisciplinaire **HAL**, est destinée au dépôt et à la diffusion de documents scientifiques de niveau recherche, publiés ou non, émanant des établissements d'enseignement et de recherche français ou étrangers, des laboratoires publics ou privés.

# Development of online separation and surfactant quantification in effluents from an Enhanced Oil Recovery (EOR) experiment

AUTHOR NAMES

Elie Ayoub[a], Perrine Cologon*[a], Marie Marsiglia[a], Jean-Baptiste Salmon[b], Christine Dalmazzone[a]

AUTHOR ADDRESS

[a] IFP Energies nouvelles, 1 et 4 avenue de Bois-Préau, 92852 Rueil-Malmaison, France

[b] Laboratoire du futur – UMR5258, 178 avenue du Dr. Schweitzer, 33600 Pessac, France

## 1. INTRODUCTION

Both the growth of global oil consumption and the decline of new conventional oil fields discoveries are observed (Bera and Mandal, 2015; Hirasaki et al., 2011; Thomas, 2008; Sheng, 2014). To match the current oil demand, reservoir recovery rate must be increased. Conventional oil production methods, namely first and secondary recovery, lead together to the recovery of around 20 to 40% of the original oil in place (Bera and Mandal, 2015; Hirasaki et al., 2011; Thomas, 2008; Sheng, 2011; Sheng, 2014). Then, the flow rate of produced oil tends towards zero, partly due to the action of capillary forces that traps the residual oil in the pores of the reservoir (Reed and Healy, 1977). The dimensionless capillary number Ca expresses the ratio of viscous drag forces to capillary forces. It has been experimentally demonstrated that the residual oil saturation in the reservoir decreases as this capillary number increases (Hakiki et al., 2017; Lake, 1989; Oughanem et al., 2015). Consequently, the action of capillary forces can be counterbalanced in several ways into the pores of the reservoir. It is possible to increase the injection velocity or the viscosity of the moving water phase by using solutions of polymers. However, these solutions are quickly limited by practical aspects related to the injection power of the pumps and the risks of rock fracking. Thus, the best way to significantly increase the capillary number is the reduction of the interfacial tension between oil and water (IFT) by several decades. This drastic reduction is obtained by using specific chemical surfactants within a tertiary recovery technique called surfactant chemical EOR (cEOR) or “surfactant flooding” (Sheng, 2011). This process consists in injecting a surfactant formulation which lowers the IFT between water and oil and thus facilitates the oil mobilization towards the producing wells (Bourrel and Schechter, 1988; Jing et al. 2021; Hirasaki et al. 2011; Sheng, 2010). In the case of sandstone reservoirs, anionic surfactants are essentially employed, due to their low tendency to adsorb on negatively charged surfaces (Chen

and Schechter, 2021). The main chemical structures are sulfates, like alkyl sulfates, alcohol ethoxy or propoxy sulfates and sulfonates, like alkyl aryl sulfonates, linear or branched alkyl benzene sulfonates, alpha-olefin or internal olefin sulfonates (Negin et al., 2017).

The formulation of the surfactants, which is the key parameter of surfactant flooding, is specifically designed to achieve ultra-low IFT (lower than $10^{-2}$ mN/m) and create a Winsor III microemulsion (WIII) with the oil at reservoir temperature (Haegel et al., 2008; Hakiki et al., 2015; Salager et al., 2013; Thomas et al., 1999). Winsor III system can be achieved by balancing the respective affinities of the hydrophobic and hydrophilic parts of the surfactants with regard to the aqueous and oily phases. The formulation design is therefore performed through salinity−scan tests, which are generally used to investigate the phase diagrams of anionic surfactant formulations (Hirasaki et al., 2011). From a practical point of view, salinity modifies the distribution of the anionic surfactant between the oil, brine and microemulsion phases (Fukumoto et al., 2016; Fukumoto et al., 2018; Salager et al., 2013). Below the optimal salinity, the surfactant is preferably soluble in brine, giving a Winsor I system (WI), consisting of an oil-in-water microemulsion in equilibrium with an excess of oil phase. At a salinity higher than the optimum, it preferably becomes soluble in the oily phase, giving a Winsor II system (WII), consisting of a water-in-oil microemulsion in equilibrium with an excess of aqueous phase. At the optimal salinity S*, the surfactant is mainly concentrated in the intermediate microemulsion phase, giving a Winsor III system consisting of a bicontinuous microemulsion in equilibrium with the excess aqueous and oily phases. It is noteworthy that the IFT is the lowest at this optimal salinity.

Most of the time, the optimal formulation can be first developed through robotic salinity-scan tests (AlSofi et al., 2021; Morvan et al., 2008). This is essentially done on model oil phases (alkanes) representative of the Equivalent Alkane Carbon Number (EACN) of the crude oil under

investigation (Queste et al., 2007). In a final step, the formulation is optimized with the real crude oil (Oukhemanou et al., 2014).

The efficiency of the designed formulation is then evaluated using a test called "coreflood experiment". This refers to a specific setup which operates on a rock sample under pressure and temperature conditions very close to those of the reservoir (Flaaten et al., 2009; Hirasaki et al., 2011; Levitt et al., 2009; Mohammadi et al., 2009). The measurement of the quantity of oil recovered and of surfactants retained on the rock makes it possible to determine the performance of the surfactant flooding process, hence the efficiency of the formulation, the environmental footprint and the profitability of the process. Evaluating the economics of the process and environmental footprint are of paramount importance. For these two parameters, it is worthwhile to recover the highest volume of oil by injecting the lowest amount of surfactants, meaning that most of surfactants must be adsorbed on the water-oil interface and only a negligible part on the rock. Therefore, the volume of oil produced by surfactant flooding and the quantity of surfactant adsorbed on the rock must be determined for each coreflood experiment. The effluents resulting from a coreflood test are complex mixtures of oil, brine and surfactants. They are generally collected in graduated cylinders or tubes as the experiment progresses. The analyses are then performed a posteriori, offline. The quantity of oil recovered is calculated from volumetric measurements (estimation of the water-to-oil volume ratio in each tube) or by a NMR analysis of the rock sample at the end of the test (Fleury and Deflandre, 2003). The presence of quite stable emulsions in the tubes induces a lower accuracy of the volumetric measurement. The concentration of surfactants is measured in the aqueous phase using various techniques such as potentiometric Hyamine titration (Liu et al., 2010), high performance liquid chromatography (HPLC), or even

UV-visible spectroscopy, though offline (Liang et al., 2021). It is noteworthy that carrying out these analyses is a tremendous challenge, especially for the determination of the surfactant concentration. A main issue concerns the presence of emulsions in the effluents that can sometimes be very stable (Dalmazzone et al., 2012). The type of these emulsions is generally oil-in-water and the presence of micronic oil droplets may interfere with the Hyamine dosage or foul the liquid chromatography column. Another trouble comes from the distribution of surfactants between the oily and aqueous phases. Depending on the experimental conditions, it is possible that the surfactants are partly trapped in the oil phase. These surfactants are not quantified in the mass balance, which may lead to an overestimation of the quantity of surfactants adsorbed or retained on the rock and consequently to the rejection of a formulation for economic and environmental reasons.

To overcome these difficulties, a micro/millifluidic device capable of treating and separating coreflood effluents online has been designed. This setup allows a relevant quantification of the surfactant concentration, online or offline. The overall approach consists in (1) performing an online dilution of the effluent with deionized water to decrease the salinity and thus promote surfactant transfer to the aqueous phase, (2) separating online the oil and the aqueous phase using a membrane, and (3) measuring the surfactant concentration.

In this paper, the designed micro/millifluidic setup is detailed. The validation of the methodology was first performed on a model system of surfactants and oil. Then, the whole micro/millifluidic assembly was tested at the outlet of a real coreflood experiment to evaluate the potential of the developed methodology in realistic and representative conditions.

## 2. MATERIALS AND METHODS

### 2.1 Chemicals

Sodium dodecylbenzenesulfonate (SDBS) (technical grade) was purchased from Sigma-Aldrich. Isobutanol ($C_4H_{10}O$) with >99% purity and n-decane ($C_{10}H_{22}$) with 99%$_{wt}$ purity were provided by Alfa Aesar. Sodium chloride (NaCl) with 99.9% purity was purchased from VWR chemicals. Organol Red was obtained from Prolabo. All compounds were used without further purification. Aqueous solutions were prepared with Milli-Q water (resistivity higher than 18.2 MΩ/cm). The industrial surfactants, Alkylglyceryl Ether Sulfonate (AGES – 33wt.% active matter) and Internal Olefin Sulfonate (IOS – 33wt.% active matter), were provided by Solvay. Arabian light crude oil, filtered over 5 μm, was chosen in this study because of its low paraffin content, avoiding clogging of the tubings at room temperature. Details of the Arabian light composition and characteristics are given in Table 1.

**Table 1.** Density and viscosity at 20°C and SARA composition of the Arabian light crude oil

| | |
|---|---|
| **Density at 20°C (g/cm3)** | 0.88 |
| **Viscosity at 20°C (mPa.s)** | 12 |
| **Saturates (wt%)** | 53.8 |
| **Aromatics (wt%)** | 32.6 |
| **Resins (wt%)** | 10.6 |
| **Asphaltenes (wt%)** | 2.7 |

### 2.2 Phase diagrams

Phase diagrams are of interest in order both to optimize EOR formulations through the identification of the optimal salinity and to treat the effluent with the appropriate methodology. While WIII microemulsions are the aim of EOR formulation design, WI microemulsions are preferred to treat the effluents as the surfactant is mainly contained in the aqueous phase for such systems.

Model fluid mixtures were prepared with decane and an aqueous phase composed of Milli-Q water, SDBS, NaCl brine and isobutanol. SDBS is a sulfonate anionic surfactant. It was selected because it is a representative surrogate for EOR surfactants due to its sulfonate polar moiety and its carbon chain length, and also because its aromatic ring makes UV-visible absorption measurement possible. Fluids representative of real systems were prepared with filtered Arabian light crude oil and an aqueous phase composed of Milli-Q water, an industrial IOS-AGES blend and NaCl brine. For both systems, salinity scans were done to determine the different Winsor zones. Microemulsions were prepared at room temperature in glass tubes using the following procedure.

- First, solutions of SDBS (16 g/L) and NaCl (200 g/L) were prepared in separate flasks. The mass of SDBS and NaCl was measured with an electronic weighing scale (AE200, Mettler Toledo) with a precision of ±0.1 mg.
- Then, 3.5 mL of the SDBS solution was added in a glass tube. Also, 0.40 mL of isobutanol (5.83 %vol. of aqueous phase) was added to ensure the dissolution of the surfactants.
- Next, the volume of the aqueous phase was adjusted to 7 mL with Milli-Q water and NaCl solutions whose respective volumes enable to achieve the set salinity (ranging from 15 to 80 g/L). At that point, the solution was carefully mixed.

- Finally, 7 mL of decane was poured along the glass tube walls, resulting in a Water to Oil Ratio (WOR) of one. The interface was gently stretched by turning the tubes upside down approximately 6 times without creating an emulsion.
- Then, the samples were left for one month at room temperature to ensure complete thermodynamic equilibrium.

Middle phases corresponding to Winsor III systems were observed for salinities ranging from 28 to 52 g/L (Figure 1). The phase transitions can be described as follows: Winsor I type microemulsion (oil-in-water) from 0 to 25 g/L NaCl, Winsor III (bicontinuous) from 28 to 52 g/L NaCl, and Winsor II (water-in-oil) from 55 to 80 g/L NaCl, in agreement with previous studies (Fukumoto et al., 2016).

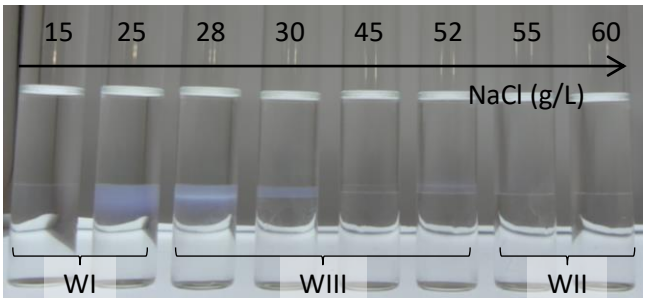


**Figure 1.** Photograph of formulated microemulsions with salt increments. Formulations are composed of water, NaCl, SDBS, isobutanol and decane. WOR is unity. WI, WII and WIII are the abbreviations of Winsor I, II and III respectively.

The same protocol was followed for the microemulsions formulated with crude oil and industrial surfactants. Decane was replaced by Arabian Light crude oil and a 4 g/L solution of IOS-AGES mixture was used instead of SDBS. Note that isobutanol was not used in this case and the WOR was set to 0.7. The samples were kept at 40 °C during four months in order to reach equilibrium. A middle phase was observed for salinities ranging from 70 to 75 g/L. Phase transitions in terms

of microemulsions can be described as follows: Winsor I (oil-in-water) from 0 to 65 g/L NaCl, Winsor III (bicontinuous) from 70 to 75 g/L NaCl, and Winsor II (water-in-oil) from 80 to 130 g/L NaCl.

### 2.3 Water-in-oil titration

Mass fraction of water in the oil phase or the microemulsion phase was measured by Karl Fischer titration. The titration was conducted with 787-KF Titrino from Metrohm with a reagent of Hydranal-Composite 5 purchased from Fluka. A weighed sample (about 10 mg) was injected into a measuring cell, and the amount of water in the sample was obtained from the volume of reagent needed to reach a significant shift in potential. All the samples were analyzed at least three times.

### 2.4 Surfactant quantification

Different techniques were used to measure the concentration of surfactant in the aqueous phase. Conventional offline analyses included Hyamine titration and High-performance liquid chromatography (HPLC).

For Hyamine titration, 1 mL of the sample was introduced in the measuring cell of the titrator (862-compact Titrosampler, Metrohm). Incremental volumes (30 µL) of titrant (Hyamine 1622-solution, Merck Millipore) were added to the sample until a shift in potential was reached.

HPLC analysis was also employed to confirm the results of Hyamine titration. Briefly, samples were injected into an Agilent 1260 Infinity system coupled to an Evaporative Light Scattering Detector (ELSD G4260B). A mixture of ammonium acetate buffer (pH = 5) and acetonitrile was used as mobile phase at a flow rate of 1 mL/min. Once separated, the surfactants were detected in

185 the ELSD (nebulization temperature: 40°C, evaporator temperature: 70°C). Both analytical
186 techniques were calibrated with standard solutions.
187 Additionally, online measurements were specifically developed: UV-visible absorption spectra
188 were acquired on an AvaSpec-ULS2048 spectrophotometer (Avantes) equipped with a deuterium-
189 halogen light source offering a wavelength range of 200 nm to 1100 nm. A micro-flow cell (18 µL
190 volume) with a 10 mm Z-design optical path was used for online measurements (Avantes).
191
192 **2.5 Micro/Millifluidic experimental setup**
193 Low pressure syringe pumps neMESYS 290N (Cetoni) were used to pump the fluids. Teflon
194 tubings from Cluzeau Info Labo (1/16'' external diameter and 762 µm internal diameter) were
195 used to connect all parts of the setup. Oil-in-water emulsions were created with two coaxial
196 capillaries. The chip was manufactured by inserting a circular capillary with a 200 µm internal
197 diameter in a square capillary of 400 µm internal width. This enables to create oil-in-water
198 emulsions at the tip of the inner capillary in the continuous aqueous phase (Utada et al., 2005).
199 Decane was colored with organol red for visualization purposes.
200 The membrane separation device is sold by Dolomite under the name "Membrane Chip Interface"
201 and is specifically designed for online liquid-liquid separation. It consists of two microfluidic glass
202 chips engraved on one side, a hydrophilic treated PTFE membrane (Part No. 3200347, Dolomite)
203 and a metal structure which seals the whole system. Each glass chip consists of a serpentine
204 channel with a length of 21.2 cm, width of 900 µm and height of 150 µm. The hydrophilic
205 membrane (25 mm in diameter and 0.2 µm nominal pore size) is sandwiched between the two
206 chips. It contains four inlets, two on each side of the membrane, to ensure the insertion of the tubes
207 allowing the connections. In our case, one of the bottom inlets was closed in order to have one

inlet on the upper side and two outlets on both sides of the membrane. Outlets are referred to as O1 and O2 for the upper and lower sides respectively. The whole system is schematically presented in Figure 2.

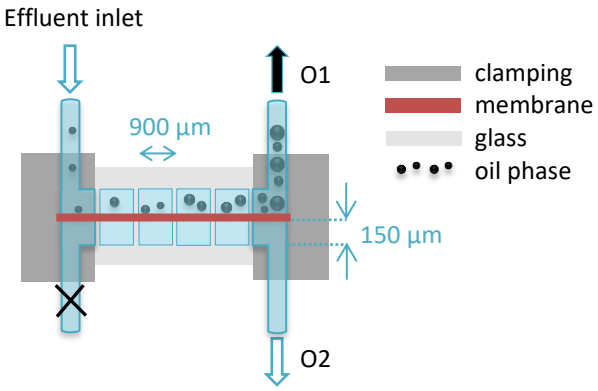


**Figure 2.** Schematic sectional view of the membrane separation device. The membrane stands in red and both outlets for the separated effluent are identified (O1 and O2). The black circles correspond to droplets of oil transported in the flowing aqueous phase (light blue).

Visualization of the fluids circulating in the system is partly possible thanks to a small opening in the metal structure.

### 2.6 Coreflood experiment

A coreflood experiment setup, designed at IFPEN and schematically presented in Figure 3, was used with a "Bentheimer" type core (38.9 mm long and 34.98 mm in diameter). This sandstone outcrop sample is often used to mimic reservoir behavior for EOR studies. The core is placed in a sleeve in a coreholder Hassler cell. An overburden pressure is then applied on the sleeve to ensure that no leak occurs between the core and the sleeve. All the experiments were carried out at a pore pressure of 10 bar and a confining pressure of 40 bar. Temperature was kept at 40°C throughout the experiment.

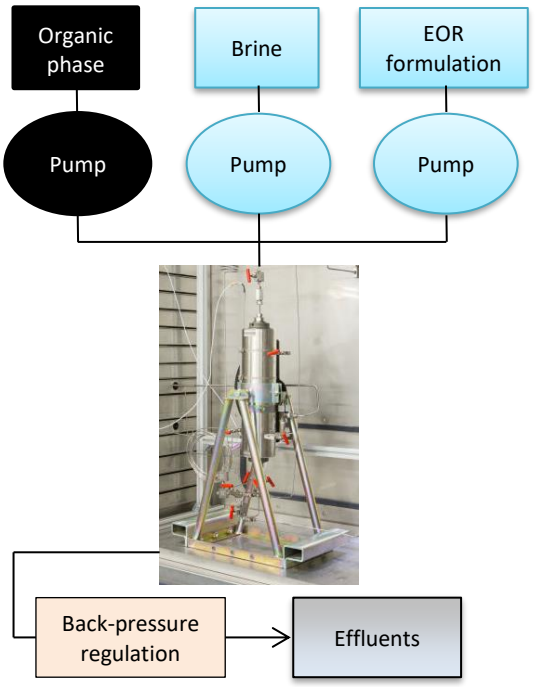


**Figure 3.** Schematic view of a coreflood experiment.

General EOR workflow has been described in details elsewhere (Moreau et al., 2010). Briefly, the following steps were applied: first of all, a forced imbibition step was performed with brine to determine the pore volume of the core (28.1 mL). In a second step, the rock was saturated with a filtered Arabian Light crude oil. Then, water injection was carried out to mimic a "waterflooding" step in order to determine the residual oil saturation (56%, i.e. 15.7 mL of oil). Finally, the formulation was injected at a flow rate of 5 mL/h for 52 hours, followed by a brine injection at 70 g/L NaCl for 50 hours.

## 3. RESULTS AND DISCUSSION

The purpose of this study is to develop a method leading to accurate measurement of surfactant concentrations in EOR effluents. Therefore, an efficient oil/water separation is needed. A dilution with water is also performed as a first step to decrease the salinity and switch the aqueous phase of the effluent to a Winsor I microemulsion because surfactants are mostly in the aqueous phase in this case.

Figure 4 displays a schematic view of the experimental setup developed to achieve these steps online. The whole assembly includes an effluent collection or generation with coaxial capillaries for model experiments to optimize the following steps (Figure 4.a), a dilution step (Figure 4.b), a membrane separation device (Figure 4.c) and an online UV-visible absorption measurement (Figure 4.d). Each step has been individually optimized, before assembling and characterizing the whole setup.

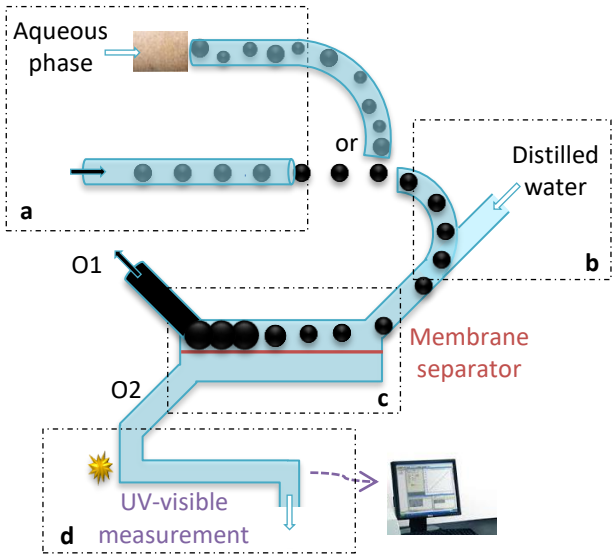


**Figure 4.** Schematic view of the experimental setup developed in this study. It includes: a. effluent collection or generation with coaxial capillaries, b. dilution with distilled water, c. membrane separation and d. UV-visible absorption measurement. The black circles show schematically oil droplets flowing in the aqueous phase (light blue).

### 3.1 Oil-in-water emulsion creation

Surrogate oil-in-water emulsions were obtained with coaxial capillaries (Figure 4.a). Water flow rate ranged from 1 to 10 mL/h which is representative of flooding conditions. Droplet size could easily be tuned by modifying the oil flow rate relatively to the one of water. For this study, the flow rate of the aqueous continuous phase was always twice the one of the organic phase. This resulted in oil droplets having a mean diameter of about 400 µm.

### 3.2 Dilution step

The effluent, either created by coaxial capillaries or collected at the outlet of the coreflood, was then diluted with Milli-Q water (Figure 4.b) using a syringe pump and a T-junction. The dilution water flow rate was equivalent to the initial flow rate of the water phase in the emulsion. This step enabled to reduce the salinity by a factor of two and thus highly increased the IFT between the aqueous phase and oil, promoting phase separation. In a first attempt, a microfluidic herringbone design was used to maximize the mixing efficiency as described in the work of Stroock et al. (2002). However, in this configuration, oil droplets were sheared into smaller droplets which limited the oil/water separation likely due to the fouling of the membrane. A simple T-junction appeared to be sufficient to dilute the effluent.

### 3.3 Membrane separation device

The oil/water separation step is represented schematically in Figure 4.c and detailed previously in Figure 2. Due to the hydrophilic nature of the membrane, the fluid in outlet O2 is expected to be mostly aqueous, whereas the fluid in outlet O1 is expected to be composed of a mixture of organic and aqueous phases.

### 3.4 Surfactant quantification

Online UV-visible absorption spectroscopy was developed in the framework of this study as a quantification technique of the surfactants in aqueous samples (Figure 4.d). UV-visible spectra obtained for different concentrations of SDBS are shown in Figure 5. The absorbance at 267 nm ($\lambda_0$) exhibited a linear relationship with SDBS concentrations (see the insert of Figure 5) according to the Beer-Lambert law, whatever the salinity (0 to 10 g/L NaCl). The choice of this wavelength to monitor SDBS is explained in the next sections.

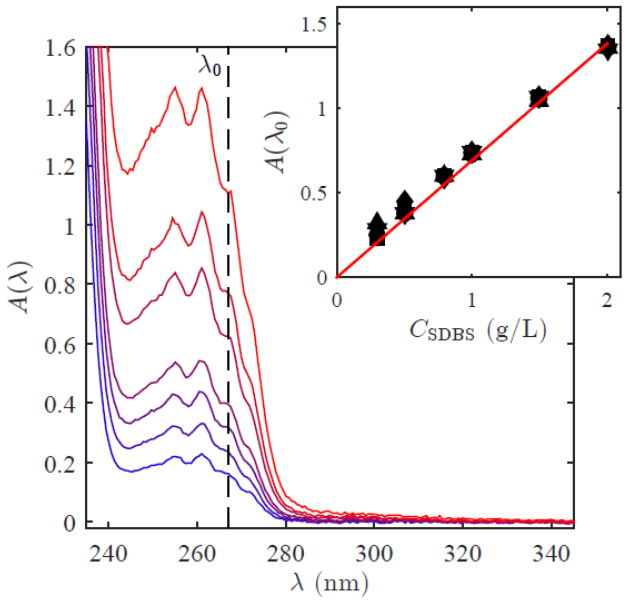


**Figure 5.** Absorbance ($A(\lambda)$) for different concentrations of SDBS in Milli-Q water at room temperature; Insert : Absorbance $A(\lambda_0)$ at the wavelength $\lambda_0 = 267$ nm chosen to monitor SDBS concentration.

### 3.5 Characterization of the membrane separation device

First, the impact of the interfacial tension between the aqueous phase and decane on the membrane separation efficiency has been studied. Therefore, different Winsor I emulsions, corresponding to

different interfacial tensions, were formed and injected directly in the separation device using the coaxial capillary device. Then, the injection was stopped to immobilize the fluids in the device, and O1 was closed. In this configuration the fluid can only flow through the membrane and the objective of this experiment was to determine the pressure at which the decane breakthrough occurs. Thus, different pressures were applied at the inlet of the device (pressure controller MFCS-EZ, Fluigent) while observing the membrane area under a stereomicroscope using the opening of the Dolomite membrane device (see insert in Figure 6 for a typical image using bright-field imaging).

At low imposed pressures, decane droplets are getting closer and some of them coalesce. At a well-defined critical transmembrane pressure drop $P_c$, one clearly sees decane droplets starting to flow through the membrane.

The interfacial tensions were measured with a Krüss SDT spinning drop tensiometer. These experiments showed that for an emulsion with an interfacial tension of 35.7±0.2 mN/m, the breakthrough pressure is about ~135 kPa. For an emulsion with an IFT of 3.6±0.4 mN/m, the breakthrough pressure decreases down to about ~22.5 kPa. And this pressure decreases further down to about ~12.5 kPa for an IFT of 1.4±0.1 mN/m. These data are plotted in Figure 6.

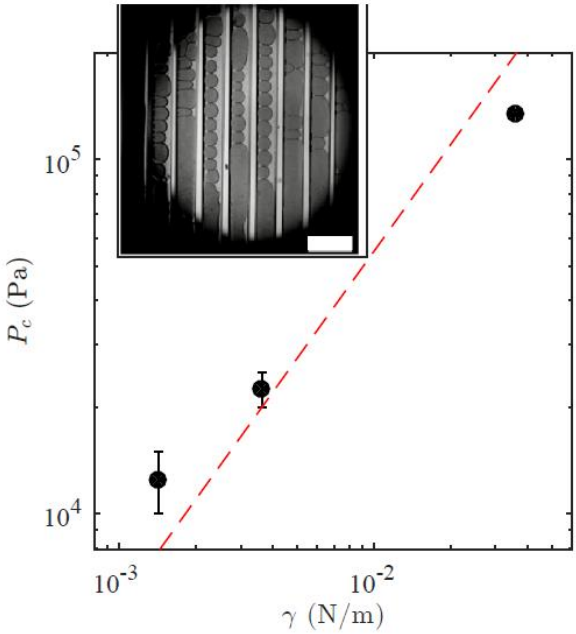


311

312 **Figure 6.** Breakthrough pressure ($P_c$) of the decane through the hydrophilic membrane versus
313 interfacial tension (γ). The red dashed line is the linear law $P_c = 2\gamma/r$ with r = 0.4µm. Insert:
314 bright-field image of the membrane separation device taken with a stereomicroscope before
315 applying pressure at the inlet.

316

317 Capillary pressure is related to the interfacial tension of the fluids according to the application of
318 Young-Laplace equation in a narrow tube of circular cross-section with a zero contact angle giving
319 the capillary pressure $2\gamma/r$, with γ the interfacial tension (N/m) and $r$ the pore radius of the
320 membrane (m). So, for a constant pore size, as a first approximation, the breakthrough pressure $P_c$
321 is proportional to the IFT. Figure 6 shows the experimental data, as well as the best linear fit of
322 the breakthrough pressure according to $P_c = 2\gamma/r$. While this relationship does not perfectly fit
323 our data, this crude estimate yields a pore size of 0.4 µm in agreement with the value given by the
324 manufacturer (0.2 µm) considering the complex geometry of the pores. Without being predictive,
325 these data allow us to determine the range of pressure for which we can be sure that the oil droplets
326 do not pass through the membrane for a given IFT.

The second characterization of the membrane separation device was to check its ability to separate an emulsion with flow rates ranging between 1 and 10.5 mL/h, in the same order of magnitude as the flow rates usually used for coreflood experiments. For this purpose, a Winsor I emulsion was created with the model system (with decane being colored with organol red for the ease of visualization) and injected in the membrane separation device at different flow rates. The fluids recovered at the two outlets were collected in flasks. Two phases were recovered at Outlet 1: a red phase and a pink one (Figure 7.b); but only one phase in Outlet 2, a pink one (Figure 7.c). The red phase of O1 is decane and the pink phase of O1 and O2 is mainly water. Its pink coloration is due to the presence of SDBS at a concentration higher than the critical micellar concentration, which allows the dispersion of organol red, insoluble in water without SDBS. Similar behaviors were observed for three different flow rates (1.5, 4.5, and 10.5 mL/h) at various salinities (0, 5, 10, and 15 g/L). Note that all the tested salinities lead to Winsor I microemulsions at thermodynamic equilibrium.

Figure 7.a shows the water percentage measured by Karl-Fisher titration, versus the emulsion flow rate at the entrance of the separation device. Water content was measured in the upper phase (red oily phase) recovered in O1 and in the aqueous phase recovered in O2. Initial fluids were also analyzed, giving the results in red ($Q$ = 0 mL/h). These values (92% ± 6% for aqueous phase – below the quantification limit for the organic phase) were in agreement with the expected concentrations.

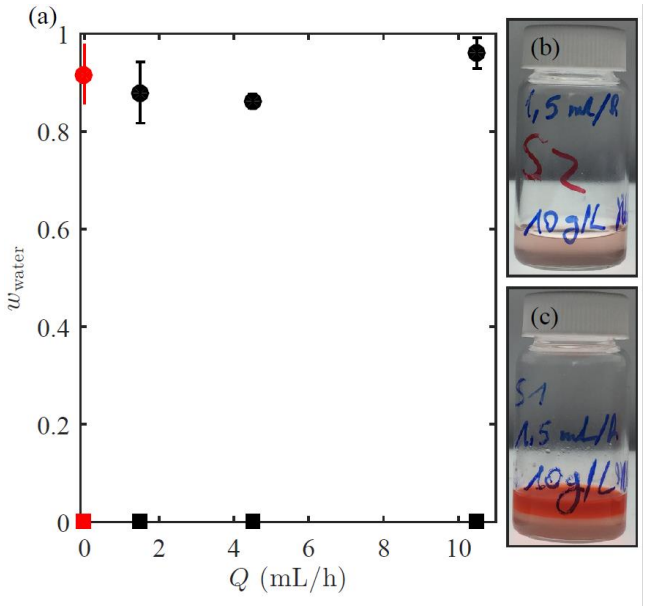


**Figure 7.** a. Water content ($w_{water}$) measured by Karl Fischer titration in the supernatant oily phase at Outlet 1 (black square) and in the aqueous phase at Outlet 2 (black circle) after separation with the membrane separation device. The water content of the initial phases is specified in red (red square for decane and red circle for the aqueous solution of SDBS). Pictures of b. Outlet 2 flask and c. Outlet 1 flask.

In O2 (black circles) water contents comprised between 88 and 96 $\%_{vol}$ were obtained, depending on the injection flow rate. Concerning the upper phase of O1, Karl Fisher titration gives the same result as the initial decane, which allows us to claim that the red phase is pure decane. Therefore, the membrane separation device leads to a >90% pure aqueous phase, which is considered satisfactory regarding the final application.

### 3.6 Characterization of the full experimental setup

This section aims at evaluating the potential of the proposed methodology for separating the organic and aqueous phases and measuring the surfactant concentration in the aqueous phase. So the complete setup was assessed, including dilution, oil/water separation and surfactant

quantification. Results obtained with either model fluids or real systems are presented in this section.

First, experiments were performed with SDBS concentrations of 0.5, 1 and 1.5 g/L, and salinities equal to 5, 10, and 15 g/L; at these salinities, Winsor I microemulsions are obtained at equilibrium. Figure 8 shows the concentrations of SDBS measured after oil/water separation at three different flow rates (1.5, 4.5, and 10.5 mL/h) for 9 formulations containing initially various amounts of NaCl and SDBS. SDBS concentrations presented in Figure 8 are the average of 8 measurements performed online with the UV-visible spectrometer at 267 nm during an hour. The measured concentrations are around 10 % lower than the expected concentrations. This difference could be due to the presence of small oil droplets that can pass through the membrane because the tested salinities lead to a Winsor I microemulsion (cf. next paragraph), leading to a different spectroscopic response. To confirm the SDBS concentration, the separated aqueous phase was also measured by Hyamine titration. The results show that the initial concentrations of 0.5±0.05, 1±0.05, and 1.5±0.04 g/L were obtained.

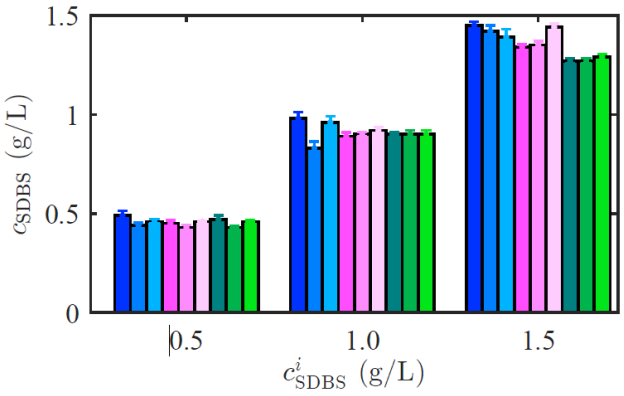


**Figure 8.** SDBS concentrations ($c_{SDBS}$) in the phase obtained in Outlet 2 measured with UV-visible spectroscopy, after separation with the membrane separation device for different flow rates (1.5, 4.5, and 10.5 mL/h from dark to light color), different salinities (5 g/L in blue, 10 g/L in pink, 15 g/L in green) and different initial SDBS concentrations ($c^i_{SDBS}$).

Both UV-visible measurements and Hyamine titration results show that in the case of the model systems, a reliable online surfactant measurement at ± 10 % can be obtained.

Furthermore, experiments were carried out to assess potential interactions between the aqueous phase containing surfactants and decane possibly resulting in changes in the UV-visible spectra. Comparisons were made between a raw 1 g/L SDBS solution in 5 g/L NaCl (blue spectrum in Figure 9) and the same solution contacted with decane for seven days at room temperature (red spectrum in Figure 9).

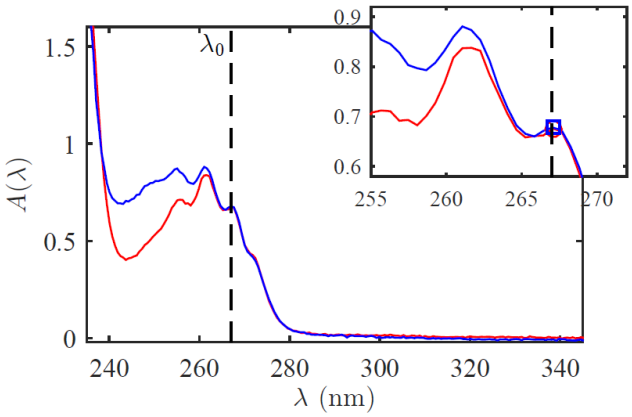


**Figure 9.** Absorbance A(λ) of a 1 g/L SDBS solution in 5 g/L NaCl before (blue) and after (red) contacting decane at room temperature.

A significant decrease in absorbance was observed in the 240-260 nm range. This might be explained by the formation of micelles in the aqueous phase, which bias the measurement. These objects have been quantified by Dynamic Light Scattering (DLS) showing that their size is around 20 nm in diameter. This observation led us to select a wavelength providing a constant signal for the SDBS quantification (267 nm, Figure 9).

Secondly, the performance of the whole experimental setup was assessed with real systems: filtered Arabian light crude oil and an aqueous phase composed of an industrial blend of surfactants at concentrations of 1, 2, and 4 g/L at a salinity of 35 g/L. At this salinity, a Winsor I microemulsion is obtained. Table 2 shows the concentrations measured with Hyamine titration at three different flow rates (1.5, 4.5, and 10.5 mL/h). The obtained concentrations are in good agreement with the expected ones.

**Table 2.** Industrial surfactant concentrations in the phase obtained in Outlet 2 measured with Hyamine titration, after separation with the membrane separation device for different flow rates (1.5, 4.5 and 10.5 mL/h) at a salinity of 35 g/L.

| Expected industrial surfactant concentration (g/L) | Measured industrial surfactant concentration | | |
|---|---|---|---|
| | 1.5 mL/h (g/L) | 4.5 mL/h (g/L) | 10.5 mL/h (g/L) |
| 1 | 1.1±0.1 | 1.1±0.1 | 1.1±0.1 |
| 2 | 2.1±0.2 | 2.1±0.2 | 2.1±0.2 |
| 4 | 3.7±0.4 | 3.7±0.4 | 3.9±0.4 |

These results confirm that the experimental setup is efficient to separate the effluents (oil-in-water emulsions), enabling accurate quantification of surfactants in the aqueous phase with offline measurements, here Hyamine titration.

Note that no online UV-visible measurement could be exploited during these experiments because the contact between crude oil and water phase containing surfactants resulted in the dispersion of compounds from the oil. Spectra were so altered in this case that no reliable quantification could be considered.

### 3.7 Coreflood Application

The implementation of our experimental setup on a coreflood experiment is presented in Figure 10.

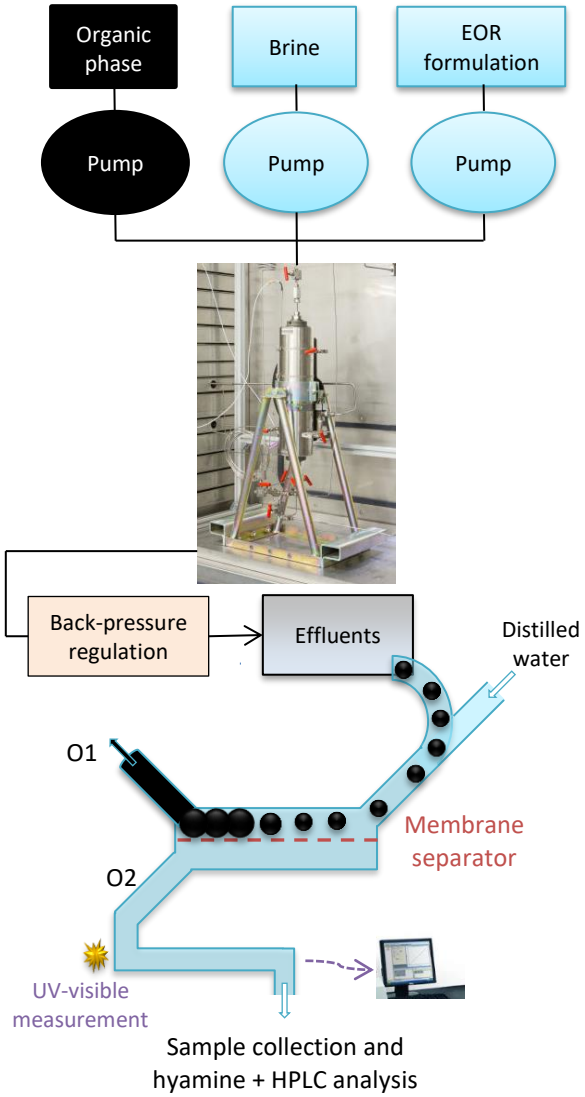


**Figure 10.** Schematic view of a coreflood experiment and downstream implementation of our experimental setup.

The formulation for surfactant flooding was optimized through a salinity scan with NaCl from a mixture of surfactants composed of 4 g/L of AGES and 4 g/L of IOS, both provided by Solvay. The optimal NaCl salinity leading to WIII microemulsions is about 70 g/L at 40°C.

While the formulation was injected, the effluents of the coreflood experiment were diverted into the microfluidic setup, located after the back-pressure regulation (Figure 10). After dilution with water and separation, the aqueous phase was pumped into to the UV-visible spectroscopy flow cell and an autosampler which collected the fluids at a frequency of 1 tube per hour for offline surfactant measurements.

Only one phase was recovered at the aqueous outlet O2 of the membrane separation device (Figure 11.b), while a mixture of oil and water was collected in the oily outlet O1. No free oil phase was seen, nor any phase separation, in the tubes of O2, even one month after the end of the experiment. Evolution of the color of the effluents collected at Outlet 2 was noticed throughout the experiment. The samples changed from transparent in the beginning to a pale yellow color that gets darker, and at the end samples gradually became transparent again. This color change could be related to the formation of an oil-in-water microemulsion with very tiny droplets (a few tens of nm droplets as shown before) that can flow through the pores of the separation membrane.

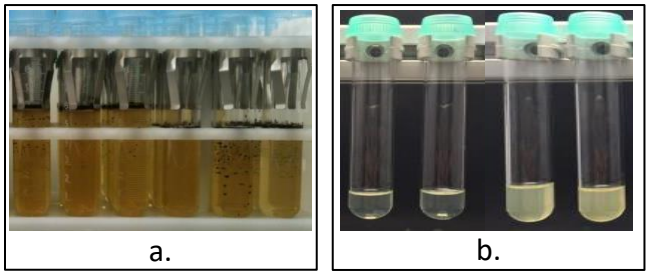


**Figure 11.** Aspect of the coreflood effluents once collected in tubes: a. without using our experimental setup, b. after using our experimental setup in the aqueous outlet (Outlet 2). A clear improvement of water quality is noticed thanks to the present setup.

This water quality is compatible with an offline determination of the surfactants by Hyamine titration and by HPLC under completely satisfactory conditions without further purification steps.

Figure 12 shows the evolution of the surfactant concentrations measured offline in the separated water phase, as a function of injected porous volume ($V_p$). Results of both analyses (Hyamine – green triangles, and HPLC – purple triangles) are quite consistent.

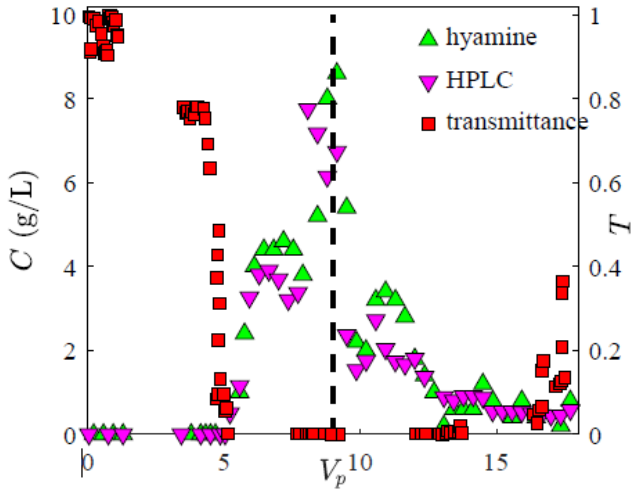


**Figure 12.** Analysis of the separated aqueous effluents from the coreflood: Evolution of the concentration of industrial surfactants (C) measured by Hyamine titration (green triangle) and HPLC (purple triangle) and evolution of the transmittance at 255 nm (red square) vs. injected porous volume ($V_p$). The dotted line stands for the end of the surfactant injection step.

It is important to note that online measurement by UV-visible spectroscopy cannot be used to quantitatively monitor surfactant concentration due to the presence of other interfering substances, as previously mentioned above. However, it can advantageously be used to follow the breakthrough of surfactants and identify their presence in specific samples generated throughout the coreflood experiment. In this case it is necessary to use the information obtained in the transmission mode. The evolution of the transmittance measured online at a wavelength of 255 nm is superimposed in Figure 12. A clear breakthrough of surfactants corresponds to the point where transmittance falls to zero. As long as the effluents contain surfactant, the transmittance value remains close to zero, and then begins to increase again as the surfactant concentration itself

becomes negligible. This information can advantageously be used to select the relevant tubes for further offline analysis.

This experiment led us to the conclusion that the experimental setup makes it possible to obtain a "clean" aqueous phase (i.e. containing no free oil) from the effluents for the quantification of surfactants. The quality of this aqueous phase enables to provide accurate results using offline techniques (Hyamine titration, HPLC) and avoids the time-consuming manual oil/water separation step. Moreover, the use of online UV-visible spectroscopy analysis allows an online monitoring of the surfactant presence which is a significant improvement over the current protocols where this information is obtained retrospectively.

## 4. CONCLUSIONS

In this work, a micro/millifluidic setup was developed with the aim of quantifying online the surfactant concentration at the outlet of a coreflood experiment. The experimental setup includes: a dilution chip to transfer the surfactants in the water phase, a membrane-based separation device, and an online UV-visible absorption spectrometer for surfactant monitoring.

The performance of the membrane separation device was first evaluated. The range of pressure for which an oily phase does not flow through the membrane was determined depending on the interfacial tension. In this pressure range, the performance of the membrane separation device was assessed with various flow rates (1 to 10 mL/h) and salinities (0 to 15 g/L NaCl). The fluid collected downstream the membrane contains around 90% water, confirming the efficiency of the device over a wide range of operating conditions.

The whole experimental setup was then successfully tested on model fluid mixtures (decane, NaCl brine and SDBS) and real systems (Arabian Light oil, NaCl brine and a mixture of IOS-AGES). The membrane separation device allowed a very efficient separation of oil-in-water emulsions and it was possible to accurately measure the concentration of surfactants in the separated aqueous phase.

The setup was finally implemented downstream a coreflood experiment to test its efficiency under industrial conditions. The oil/water separation proved to be efficient, providing an aqueous phase compatible with further offline analyses like potentiometric Hyamine titration or HPLC. The direct online surfactant measurement with UV-visible spectroscopy was unfortunately prevented by the presence of interferences due to the contact with crude oil. However, the transmittance signal could advantageously be exploited to continuously follow the breakthrough of surfactants and target the relevant samples for offline analyses, which is clearly an improvement compared to classical protocols. Table 3 summarizes the upgrading reached thanks to the experimental setup developed in the present study.

**Table 3.** Improvements obtained in the present study, compared to classical monitoring approaches

| | Classical methods | Improvements obtained in the present study |
|---|---|---|
| Oil/water separation | Offline gravity separation | Online membrane separation |
| Surfactant analysis | Offline | Online/Offline |
| Surfactant analysis technique | Potentiometric titration | UV-visible (online) or HPLC (offline) |
| Measurement accuracy | Low: (1) poor oil/water separation leading to high uncertainties, (2) part of the surfactant remains trapped in the oil phase and is therefore not quantified. | Greatly improved: (1) very low residual oil amounts, (2) the dilution step enables to transfer all surfactant in the aqueous phase. |

## AUTHOR INFORMATION

### Author Contributions

The manuscript was written through contributions of all authors. All authors have given approval to the final version of the manuscript.

## ACKNOWLEDGMENT

Solvay is acknowledged for providing the industrial surfactants.

512 REFERENCES

513 AlSofi A.M., Miralles V., Rousseau D., Dokhon W.A. (2021) An all-inclusive laboratory
514 workflow for the development of surfactant/polymer formulations for EOR in harsh
515 carbonates, Journal of Petroleum Science and Engineering 200, 108131. DOI:
516 https://doi.org/10.1016/j.petrol.2020.108131
517 Bera A., Mandal A. (2015) Microemulsions: A novel approach to enhanced oil recovery: a review,
518 J Petrol Explor Prod Technol 5, 3, 255–268. DOI: https://doi.org/10.1007/s13202-014-0139-
519 5
520 Bourrel, M. and Schechter, R.S. (ed.) (1988) Microemulsions and Related Systems: Formulation,
521 Solvency and Physical Properties, Marcel Dekker, New York. DOI:
522 https://doi.org/10.1080/01932699008943264
523 Chen W. and Schechter D.S. (2021) Surfactant selection for enhanced oil recovery based on
524 surfactant molecular structure in unconventional liquid reservoirs, Journal of Petroleum
525 Science and Engineering 196, 107702. DOI: https://doi.org/10.1016/j.petrol.2020.107702
526 Dalmazzone C., Noïk C., Argillier J.-F. (2012) Impact of Chemical Enhanced Oil Recovery on the
527 Separation of Diluted Heavy Oil Emulsions, Energy Fuels 26, 6, 3462–3469. DOI:
528 https://doi.org/10.1021/ef300083z
529 Flaaten A.K., Nguyen Q.P., Pope G.A., Zhang J. (2009) A Systematic Laboratory Approach to
530 Low Cost, High Performance Chemical Flooding, SPE reservoir Evaluation and Engineering
531 12, 5, 713–723. DOI: https://doi.org/10.2118/113469-PA
532 Fleury M., Deflandre F. (2003) Quantitative Evaluation of Porous Media Wettability Using NMR
533 Relaxometry, Magnetic Resonance Imaging 21, Special Issue // 3-4, 385–387. DOI:
534 10.1016/s0730-725x(03)00145-0
535 Fukumoto A., Dalmazzone C., Frot D., Barré L., Noïk C. (2016) Investigation on Physical
536 Properties and Morphologies of Microemulsions formed with Sodium Dodecyl
537 Benzenesulfonate, Isobutanol, Brine, and Decane, Using Several Experimental Techniques,
538 Energy Fuels 30, 6, 4690–4698. DOI: https://doi.org/10.1021/acs.energyfuels.6b00595
539 Fukumoto A., Dalmazzone C., Frot D., Barré L., Noïk C., Dalmazzone C. (2018) Characterization
540 of Complex Crude Oil Microemulsions-DSC Contribution, Oil & Gas Science and
541 Technology - Rev. IFP Energies nouvelles 73, 4, 3. DOI:
542 https://doi.org/10.2516/ogst/2017039

543 Haegel F.-H., Lopez J.C., Salager J.L., Engelskirchen S. (2008) Microemulsions in Large Scale
544 Applications, in Microemulsions: Background, New Concepts, Applications, Perspectives,
545 Stubenrauch C. (ed.), Wiley_Blackwell.
546 Hakiki F., Ayuda Maharsi D., Marhaendrajana T. (2015) Surfactant-Polymer Coreflood
547 Simulation and Uncertainty Analysis Derived from Laboratory Study, Journal of Engineering
548 and Technological Sciences 47, 6, 706-724. DOI:
549 https://doi.org/10.5614/j.eng.technol.sci.2015.47.6.9
550 Hakiki F., Aditya A., Ulitha D.T., Shidqi M., Adi W.S., Wibowo K.H., Barus M. (2017) Well and
551 Inflow Performance Relationship for Heavy Oil Reservoir under Heating Treatment, SPE
552 186187 in SPE/IATMI Asia Pacific Oil & Gas Conference and Exhibition, Jakarta, Indonesia,
553 October 2017. DOI: https://doi.org/10.2118/186187-MS
554 Hirasaki G.J., Miller C.A., Puerto M. (2011) Recent Advances in Surfactant EOR, SPE Journal
555 16, 04, 889–907. DOI: https://doi.org/10.2118/115386-PA
556 Jing W., Fu S., Zhang L., Li A., Ren X., Xu C., Gao Z. (2021) Pore scale experimental and
557 numerical study of surfactant flooding for enhanced oil recovery, Journal of Petroleum
558 Science and Engineering 196, 107999. DOI: https://doi.org/10.1016/j.petrol.2020.107999
559 Lake L.W. (ed.) (1989) Enhanced Oil Recovery, Prentice Hall, Englewood Cliffs, N.J. ISBN:
560 0132816016, 9780132816014.
561 Levitt D.B., Jackson A.C., Heinson C., Britton L.N., Malik T., Dwarakanath V., and Pope G.A.
562 (2009) Identification and Evaluation of High-Performance EOR Surfactants, SPE reservoir
563 Evaluation and Engineering 12, 2, 243–253. DOI: https://doi.org/10.2118/100089-PA
564 Liang T, Zhao X., Yuan S., Zhu J., Liang X., Li X., Zhou F. (2021) Surfactant-EOR in tight oil
565 reservoirs: Current status and a systematic surfactant screening method with field
566 experiments, Journal of Petroleum Science and Engineering 196, 108097. DOI:
567 https://doi.org/10.1016/j.petrol.2020.108097
568 Liu S., Li R.F., Miller C.A., Hirasaki G.J. (2010) Alkaline/Surfactant/Polymer Processes: Wide
569 Range of Conditions for Good Recovery, SPE Journal 15, 02, 282–293. DOI:
570 https://doi.org/10.2118/113936-PA
571 Mohammadi H., Delshad M., Pope G.A. (2009) Mechanistic Modeling of ASP Floods, SPE
572 reservoir Evaluation and Engineering 2, 4, 518–527. DOI: https://doi.org/10.2118/110212-PA

573 Moreau P., Morvan M., Rivoal P., Bazin B., Douarche F., Argillier J.-F., Tabary R. (2010) An
574 Integrated Workflow for Chemical EOR Pilot Design: SPE paper 129865, in SPE Improved
575 Oil Recovery Symposium, Tulsa, Oklahoma, USA, 24-28 April, SPE (ed.). DOI:
576 https://doi.org/10.2118/129865-MS
577 Morvan M., Koetitz R., Moreau P., Pavageau B., Rivoal P., Roux B. (2008) A combinatorial
578 approach for identification of performance EOR surfactants: SPE 113705, in SPE/DOE
579 Improved Oil Recovery Symposium, Tulsa, Oklahoma, USA, 19-23 April, SPE (ed.). DOI:
580 https://doi.org/10.2118/113705-MS
581 Negin C., Ali S., Xie Q. (2017) Most common surfactants employed in chemical enhanced oil
582 recovery, Petroleum 3, 2, 197–211. DOI: https://doi.org/10.1016/j.petlm.2016.11.007
583 Oughanem R., Youssef S., Bauer D., Peysson Y., Maire E., Vizika O. (2015) A Multi-Scale
584 Investigation of Pore Structure Impact on the Mobilization of Trapped Oil by Surfactant
585 Injection, Transp Porous Med 109, 3, 673–692. DOI: 10.1007/s11242-015-0542-5
586 Oukhemanou F., Courtaud T., Morvan M., Moreau P., Mougin P., Féjean C., Pedel N., Bazin B.,
587 Tabary R., Tabary R. (2014) Alkaline-Surfactant-Polymer Formulation Evaluation In Live Oil
588 Conditions: The Impact Of Temperature, Pressure And Gas On Oil Recovery Performance:
589 SPE 169130, in SPE Improved Oil Recovery Symposium, Tulsa, Oklahoma, USA, 12-16
590 April, SPE (ed.). DOI: https://doi.org/10.2118/169130-MS
591 Queste S., Salager J.L., Strey R., Aubry J.M. (2007) The EACN scale for oil classification revisited
592 thanks to fish diagrams, Journal of colloid and interface science 312, 1, 98–107. DOI:
593 10.1016/j.jcis.2006.07.004
594 Reed R.L., Healy R.N. (1977) Some physicochemical aspects of microemulsion flooding: A
595 Review, in Improved Oil Recovery by Surfactant and Polymer Flooding, D. O. Shah and R.
596 S. Schechter (ed.), Academic Press, pp. 383–437.
597 Salager J.-L., Forgiarini A.M., Bullón J. (2013) How to Attain Ultralow Interfacial Tension and
598 Three-Phase Behavior with Surfactant Formulation for Enhanced Oil Recovery: A Review.
599 Part 1. Optimum Formulation for Simple Surfactant–Oil–Water Ternary Systems, J Surfact
600 Deterg 16, 4, 449–472. DOI: 10.1007/s11743-013-1470-4
601 Sheng J.J. (2010) Optimum phase type and optimum salinity profile in surfactant flooding, Journal
602 of Petroleum Science and Engineering 75, 1-2, 143–153. DOI:
603 https://doi.org/10.1016/j.petrol.2010.11.005

Sheng J. (2011) Modern chemical enhanced oil recovery: Theory and practice, Gulf Professional Pub., Amsterdam Boston. ISBN: 978-1-85617-745-0.

Sheng J.J. (2014) A comprehensive review of alkaline-surfactant-polymer (ASP) flooding, Asia-Pac. J. Chem. Eng. 9, 471-489. DOI: https://doi.org/10.1002/apj.1824

Stroock A.D., Dertinger S.K.W., Ajdari A., Mezic I., Stone H.A., Whitesides G.M. (2002) Chaotic mixer for microchannels, Science 295, 5555, 647–651. DOI: 10.1126/science.1066238

Thomas S., Farouq Ali S.M. (1999) Status and Assessment of Chemical Oil Recovery Methods, Energy Sources 21, 1-2, 177–189. DOI: https://doi.org/10.1080/00908319950015046

Thomas S. (2008) Enhanced Oil Recovery - An Overview, Oil & Gas Science and Technology - Rev. IFP 63, 1, 9–19. DOI: https://doi.org/10.2516/ogst:2007060

Utada A.S., Lorenceau E., Link D.R., Kaplan P.D., Stone H.A., Weitz D.A. (2005) Monodisperse double emulsions generated from a microcapillary device, Science 308, 5721, 537–541. DOI: 10.1126/science.1109164